Redox-mediated regulation of an evolutionarily conserved cross-β structure formed by the TDP43 low complexity domain

Yi Lin[a,1], Xiaoming Zhou[a], Masato Kato[a,b], Daifei Liu[a], Sina Ghaemmaghami[c], Benjamin P. Tu[a], and Steven L. McKnight[a,2]

[a]Department of Biochemistry, University of Texas Southwestern Medical Center, Dallas, TX 75390-9152; [b]Institute for Quantum Life Science, National Institutes for Quantum and Radiological Science and Technology, 263-8555 Chiba, Japan; and [c]Department of Biology, University of Rochester, Rochester, NY 14627

Contributed by Steven L. McKnight, September 9, 2020 (sent for review June 15, 2020; reviewed by Vadim N. Gladyshev, Arthur L. Horwich, and Peter St George-Hyslop)

A methionine-rich low complexity (LC) domain is found within a C-terminal region of the TDP43 RNA-binding protein. Self-association of this domain leads to the formation of labile cross-β polymers and liquid-like droplets. Treatment with H_2O_2 caused phenomena of methionine oxidation and droplet melting that were reversed upon exposure of the oxidized protein to methionine sulfoxide reductase enzymes. Morphological features of the cross-β polymers were revealed by H_2O_2-mediated footprinting. Equivalent TDP43 LC domain footprints were observed in polymerized hydrogels, liquid-like droplets, and living cells. The ability of H_2O_2 to impede cross-β polymerization was abrogated by the prominent M337V amyotrophic lateral sclerosis-causing mutation. These observations may offer insight into the biological role of TDP43 in facilitating synapse-localized translation as well as aberrant aggregation of the protein in neurodegenerative diseases.

low-complexity sequence | cross-beta polymers | TDP-43 | redox sensor | neurodegenerative disorders

A protein designated Tar DNA-binding protein 43 (TDP43) has been the focus of extensive research owing to its propensity to aggregate in the cytoplasm or axoplasm of neurons in patients suffering from neurodegenerative diseases (1). In a bold and unbiased series of experiments, Lee and coworkers discovered TDP43 aggregates in the brain tissue of disease-bearing patients (2). Over the past decade, TDP43 has emerged as one of the most intensively studied proteins in the field of neurodegenerative diseases. The normal biological role of TDP43 has also captured interest owing to its role in the formation of neuronal granules. The TDP43 protein helps facilitate messenger RNA (mRNA) maturation, mRNA export from nuclei, formation of neuronal granules, and localized, dendritic translation proximal to active synapses (3–6).

TDP43 contains a structured amino-terminal domain that facilitates homotypic oligomerization (7), two prototypic RRM domains (8), and a carboxyl-terminal domain of low sequence complexity believed to function either in the absence of structural order (9) or via formation of a labile α-helix (10). Human genetic studies of patients suffering from amyotrophic lateral sclerosis (ALS), fronto-temporal dementia (FTD), and other neurodegenerative diseases have led to the discovery of missense mutations clustered within the C-terminal low complexity (LC) domain of TDP43 (11). It is believed, and in some cases known, that these mutations favor pathological aggregation driven by the TDP43 LC domain. TDP43 aggregation has further been observed in the cytoplasm of neurons under disease conditions driven by expansion of a polyglutamine region of ataxin-2 (12) or a hexanucleotide repeat localized within the first intron of the C9orf72 gene (13).

The LC domains of FUS, many different hnRNP proteins, and many different DEAD box RNA helicase enzymes are typified by the abundant distribution of tyrosine and/or phenylalanine residues. Numerous studies have given evidence that these aromatic residues are important for self-associative interactions that allow for phase transition of LC domains in the form of hydrogels or liquid-like droplets (14, 15). The LC domain of human TDP43 contains one tyrosine residue and five phenylalanine residues but is distinguished from prototypic LC domains by the presence of 10 evolutionarily conserved methionine residues. Here, we show that the TDP43 LC domain self-assembles in a manner specifying a redox-sensitive molecular complex. TDP43 polymers are sensitive to H_2O_2-mediated disassembly wherein methionine residues are converted to the methionine sulfoxide state. In this regard, the behavior and biological properties of the TDP43 LC domain are reminiscent of the LC domain specified by the yeast ataxin-2 protein (16, 17). We hypothesize that both the ataxin-2 and TDP43 LC domains assemble into oligomeric structures specifying redox sensors that constitute proximal receptors to the action of reactive oxygen species.

Significance

The TDP43 RNA binding protein is frequently aggregated in the brain tissue of patients suffering from neurodegenerative diseases. Human genetic studies of patients suffering from ALS have identified scores of missense mutations clustered within a localized region of the TDP43 protein. This region is of low sequence complexity and has been thought to exist in a state of structural disorder under conditions of proper TDP43 function. The present study gives evidence that the low complexity domain of TDP43 self-associates into a specific structural conformation that may be important to its normal biological function. Unlike prototypic low complexity domains, that of TDP43 is methionine-rich. Evidence is presented suggestive of the utility of these methionine residues in oxidation-mediated regulation of TDP43 function.

Author contributions: Y.L., X.Z., M.K., S.G., B.P.T., and S.L.M. designed research; Y.L., X.Z., M.K., D.L., and S.G. performed research; Y.L., X.Z., M.K., D.L., and S.G. analyzed data; and Y.L., X.Z., M.K., S.G., and S.L.M. wrote the paper.

Reviewers: V.N.G., Brigham and Women's Hospital; A.L.H., Yale University School of Medicine; and P.S.G.-H., University of Toronto.

The authors declare no competing interest.

[1]Present address: Tsinghua-Peking Center for Life Science, IDG/McGovern Institute for Brain Research, School of Life Sciences, Tsinghua University, 100084 Beijing, China.

[2]To whom correspondence may be addressed. Email: steven.mcknight@utsouthwestern.edu.

This article contains supporting information online at https://www.pnas.org/lookup/suppl/doi:10.1073/pnas.2012216117/-/DCSupplemental.

First published November 3, 2020.

Results

Recombinant proteins linking the terminal 152 amino acid residues of TDP43 to maltose binding protein (MBP) and/or a 6×-histidine tag were expressed in *Escherichia coli*, purified and incubated under physiologic conditions of monovalent salt and neutral pH (*Materials and Methods*). Both fusion proteins were observed to transition into a gel-like state in a manner temporally concordant with the formation of homogeneous polymers as observed by transmission electron microscopy (EM) (*SI Appendix*, Fig. S1*A*). Lyophilized gel samples were evaluated by X-ray diffraction, yielding prominent cross-β diffraction rings at 4.7 and 10 Å (*SI Appendix*, Fig. S1*E*). When analyzed by semidenaturing agarose gel electrophoresis, the amyloid-like polymers formed from the TDP43 LC domain dissolved such that the protein migrated in the monomeric state (*SI Appendix*, Fig. S1*B*). As such, we conclude that the TDP43 LC domain is capable of forming labile, cross-β polymers similar to polymers formed by the LC domains of the FUS protein (14), various hnRNP proteins (15), and the head domains of various intermediate filament proteins (18).

Prior to gelation, solutions containing the 6×His-tagged LC domain of TDP43 became cloudy (*SI Appendix*, Fig. S1*C*). Light microscopic examination of the solutions revealed uniform droplets 2–10 μm in diameter. Recognizing that the TDP43 LC domain contains 10 evolutionarily conserved methionine residues, we exposed the observed droplets to varying concentrations of hydrogen peroxide (H_2O_2). Droplet melting was initially observed at 0.06% (19.6 mM) H_2O_2, and droplets fully disappeared at 0.3% (98 mM) H_2O_2 (Fig. 1*A*). By contrast, no evidence of melting was observed for liquid-like droplets formed from the LC domain of FUS even upon exposure to 1% H_2O_2, presumably because only one methionine is present in this sequence (17). Upon resolving the protein samples variously exposed to H_2O_2 by sodium dodecyl sulfate polyacrylamide gel electrophoresis (SDS-PAGE), the TDP43 protein was observed to migrate more slowly as a consequence of methionine oxidation (Fig. 1*B*). Direct evidence of H_2O_2-mediated methionine oxidation of the TDP43 LC domain was confirmed by mass spectrometry as will be shown subsequently in this work.

In addition to melting liquid-like droplets formed upon self-association of the TDP43 LC domain, H_2O_2 also disassembled hydrogel polymers formed by the TDP43 LC domain. As shown in *SI Appendix*, Fig. S2, overnight incubation of cross-β polymers formed from a fusion protein linking MBP to the TDP43 LC domain led to polymer disassembly. The same conditions of incubation with H_2O_2 failed to disassemble cross-β polymers made from either a GFP fusion protein linked to the LC domain of the FUS RNA-binding protein, or an mCherry fusion protein linked to the LC domain of the hnRNPA2 RNA-binding protein.

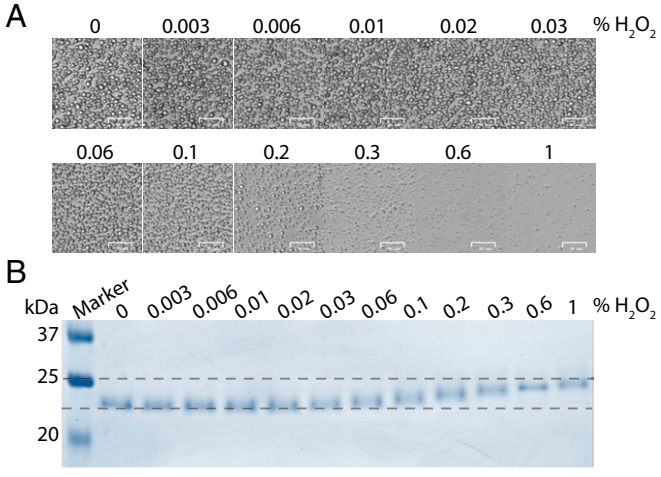

Fig. 1. H_2O_2-mediated oxidation of the TDP43 low complexity domain. (*A*) Liquid-like droplets of TDP-43 LC domain were exposed to indicated concentrations of H_2O_2 for 1 h. (Scale bar, 25 μm.) (*B*) Coomassie-stained SDS-PAGE analysis of a purified sample of the TDP43 LC domain after exposure to varied concentrations of H_2O_2 ranging from 0% (left) to 1% (right).

Assuming that liquid-like droplets formed from the TDP43 LC domain might melt as a consequence of methionine oxidation, we tested for droplet reformation upon addition of the MsrA and MsrB methionine sulfoxide reductase enzymes that are known to reduce the two stereoisomeric forms of methionine sulfoxide (19). H_2O_2-mediated oxidation was first quenched by addition of sodium sulfite (Na_2SO_3). We then added the MsrA and MsrB enzymes and supplemented the reaction with thioredoxin, thioredoxin reductase, and NADPH. These agents allow for sequential steps of reduction of the otherwise oxidized TDP43 methionine residues; reduction of the oxidized MsrA and MsrB enzymes; reduction of oxidized thioredoxin; reduction of oxidized thioredoxin reductase; and terminal conversion of NADPH to $NADP^+$. The combination of the five reagents allowed reformation of liquid-like droplets (Fig. 2*A*) and returned the migration pattern of the TDP43 protein to that of the starting protein as deduced by SDS gel electrophoresis (Fig. 2*B*). Removal of either of the two methionine sulfoxide reductase enzymes partially impeded droplet reformation and partially restored the more rapid migration of the TDP43 substrate protein on SDS gels. By contrast, droplet reformation was fully eliminated upon removable of: 1) both Msr enzymes; 2) thioredoxin; 3) thioredoxin reductase; or 4) NADPH.

A method of H_2O_2-mediated footprinting was used to characterize cross-β polymers formed from the TDP43 LC domain (*SI Appendix*, Fig. S3). Following concepts articulated in a recent study of proteome-wide susceptibility of cellular proteins to H_2O_2-mediated oxidation (20), it was reasoned that regions of the TDP43 LC domain directly involved in the formation of structural order might be partially immune to oxidation relative to regions remaining in a state of molecular disorder. Hydrogel preparations of the TDP43 LC domain were exposed for 5 min to a buffer supplemented with varying concentrations of H_2O_2. The reaction was quenched by the addition of 300 mM Na_2SO_3, desalted to remove the excess sodium sulfite, denatured in 6 M guanidine HCl, and fully oxidized by exposure to 1% ^{18}O-labeled H_2O_2. The terminal step of saturation oxidation with ^{18}O-labeled H_2O_2 served two purposes. First, it ensured that no spurious ^{16}O oxidation could take place during mass spectrometry sample preparation and analysis. Second, it allowed for accurate quantitation of the fractional oxidation from mass spectrometry data by measuring the $^{18}O/^{16}O$ ratio for individual methionine residues (20). The protein was then fragmented to completion with chymotrypsin and subjected to mass spectrometry as a means of determining the ratio of ^{18}O to ^{16}O for each of the 10 methionine residues resident within the TDP43 LC domain (*Materials and Methods*).

We interpret low $^{18}O/^{16}O$ ratios equivalent to fully denatured TDP43 to be reflective of unstructured methionine residues, and high $^{18}O/^{16}O$ ratios to be reflective of methionine residues that might be involved in formation of cross-β structure. Fig. 3 shows a varied pattern of protection for the 10 methionine residues localized within the TDP43 LC domain. This pattern corresponds to an H_2O_2 "footprint" of the TDP43 LC domain observed in highly polymeric, hydrogel samples of the protein (Fig. 3 *A*, *Left*). A footprint of protein present in liquid-like droplets is shown in Fig. 3*A*, *Center*. These similar footprints predict methionine residues M322 and M323 to be substantially protected from H_2O_2-mediated oxidation. More modest levels of

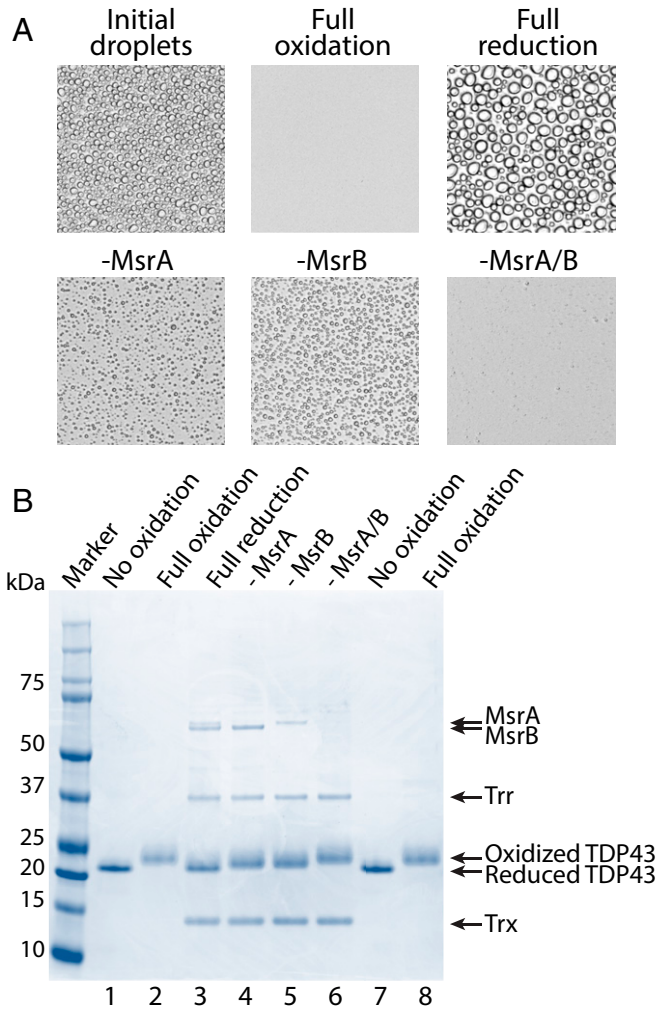

Fig. 2. Reduction of the oxidized TDP43 LC domain by two methionine sulfoxide reductase enzymes revives formation of liquid-like droplets. (*A*) Photographs of liquid-like droplets formed by untreated, recombinant TDP43 LC domain (*Upper Left*), H_2O_2-oxidized protein (*Upper Center*), protein exposed to both MsrA and MsrB methionine sulfoxide reductase enzymes, thioredoxin, thioredoxin reductase, and NADPH (*Upper Right*). Lower three images show droplets formed from enzymatic reduction reactions missing only MsrA (*Lower Left*), only MsrB (*Lower Center*), or both methionine sulfoxide reductase enzymes (*Lower Right*). (*B*) An SDS-PAGE used to resolve electrophoretic migration patterns of the TDP43 LC domain. H_2O_2-mediated oxidation retarded the migration of the TDP43 LC domain (lane 2). Incubation of the oxidized protein with both MsrA and MsrB methionine sulfoxide reductase enzymes, thioredoxin, thioredoxin reductase, and NADPH restored the migration pattern to that of the reduced protein (lane 3). Removal of either Msr enzyme led to partial restoration of the electrophoretic mobility of the protein (lanes 4 and 5). Removal of both Msr enzymes failed to alter the electrophoretic pattern of the oxidized protein (lane 6). Lanes 7 and 8 were loaded with fully reduced and fully oxidized proteins, respectively.

protection were observed for methionine residues M336, M337, and M339. The two methionine residues located closest to the carboxyl terminus of the protein (M405 and M414), and the two methionine residues located on the amino terminal side of the LC domain (M307 and M311), were poorly protected from H_2O_2-mediated oxidation in both hydrogel and liquid-like droplet samples of the TDP43 LC domain.

Moving from test tube studies of recombinant protein to living cells, we used CRISPR methods to insert both a 3×Flag epitope tag and green fluorescent protein (GFP) onto the amino terminus of the endogenous TDP43 protein of HEK293 cells (*Materials and Methods*). Live-cell imaging of the GFP-tagged protein revealed punctate nuclear staining (*SI Appendix*, Fig. S4) consistent with numerous published studies of TDP43 (21, 22). In order to probe for the presence or absence of structural order within the TDP43 LC domain in living cells, we exposed the CRISPR-modified HEK293 cells for 5 min to varying levels of H_2O_2. The cells were then frozen in liquid nitrogen and powdered using a cryo-mill instrument (*Materials and Methods*). Cryo-mill powder was resuspended in lysis buffer and separated into soluble and insoluble fractions by centrifugation. As shown in *SI Appendix*, Fig. S5, graded increases in H_2O_2 led to graded changes in the ratio of soluble/insoluble TDP43. In the absence of added H_2O_2, western blot analysis revealed that ∼50% of the cellular TDP43 remained in an insoluble state. This amount of insoluble protein was reduced in a graded manner upon exposure of cells to 0.01%, 0.03%, or 0.1% H_2O_2 and fully eliminated from cells exposed to either 0.3% or 1% H_2O_2. These H_2O_2-mediated decreases in the insoluble fraction of TDP43 were reciprocally balanced by increases in the amount of soluble protein.

Recognizing that H_2O_2-mediated oxidation of TDP43 might influence its solubility, we resuspended cryo-mill powder in lysis buffer supplemented with 4 M urea. Addition of the chaotropic agent allowed for complete solubilization of TDP43 under conditions compatible with immunoprecipitation using anti-Flag antibodies. We thus treated growing cells for 5 min with 0.1% ^{16}O-labeled H_2O_2, prepared cryo-mill lysate, solubilized the powder with lysis buffer containing 4 M urea, and immunoprecipitated the Flag-tagged TDP43 protein. Postimmunoprecipitation, the protein was denatured in 5% SDS and exposed to 1% ^{18}O-labeled H_2O_2 in order to saturate oxidation of all methionine residues within the TDP43 LC domain. The sample was quenched with sodium sulfite, desalted, chymotrypsin digested to completion and evaluated by mass spectrometry to measure the $^{18}O/^{16}O$ ratio of each of the 10 methionine residues within the TDP43 LC domain. As shown in Fig. 3*A*, *Right*, the oxidation footprint observed for cellular TDP43 was similar to the footprints observed in both hydrogel and liquid-like droplet preparations of the recombinant protein.

To more carefully investigate the methionine oxidation footprint observed in cells, we performed H_2O_2 dose–response analyses using two methodologies. In the first of the two cases, cells were exposed to 0.03%, 0.1%, or 0.3% H_2O_2 and analyzed by the same methods of shotgun mass spectrometry as described above. As shown in *SI Appendix*, Fig. S6, graded increases in the level of ^{16}O methionine oxidation were observed as a function of graded increases in H_2O_2 dose. Cellular material was subsequently processed identically for use in an independent series of experiments wherein targeted methods of mass spectrometry were employed instead of shotgun mass spectrometry (*Materials and Methods*). Additionally, as analyzed by the targeted mass spectrometry approach, we performed each experiment in triplicate. The combination of considerably more robust data availed by the use of the targeted mass spectrometry approach, coupled with three biological replicates, offers enhanced confidence that the various methionine residues localized within the TDP43 LC domain indeed vary in a reproducible manner with respect to sensitivity to H_2O_2-mediated oxidation. In all experiments, methionine residues 322 and 323 were demonstrably more resistant to oxidation relative to the eight other methionines within the TDP43 LC domain.

The location of the methionine oxidation footprint of TDP43, as defined by the boundaries of methionine residues 322 and 339, is highlighted in yellow upon the sequences of the TDP43 LC

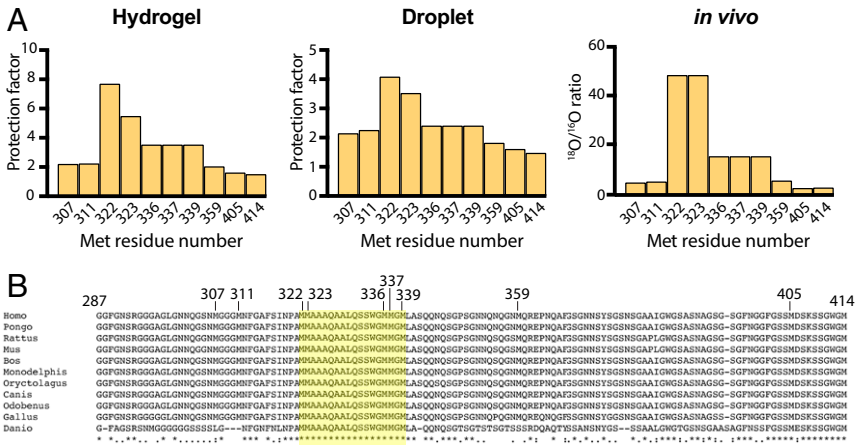

Fig. 3. H_2O_2-mediated footprints of TDP43 protein present in hydrogel samples, liquid-like droplets, and HEK293 cells. (*A*) For recombinant protein samples used to form hydrogels (*Left*) and liquid-like droplets (*Center*), samples were exposed to varying concentrations of H_2O_2 for 30 min. After quenching reactions with sodium sulfite, samples were denatured in 6 M guanidine hydrochloride and exposed for 30 min to a 0.5% solution of ^{18}O-labeled H_2O_2. The $^{18}O/^{16}O$ ratio for each methionine residue within the TDP43 LC domain was then determined from chymotrypsin digested samples by mass spectrometry and normalized relative to monomeric protein to determine protection factors (*Materials and Methods*). For cellular TDP43 (*Right*), HEK293 cells were exposed for 5 min to 0.1% H_2O_2. Cells were cryo-mill disrupted and solubilized in 4 M urea. Flag-tagged TDP43 was recovered by immunoprecipitation, exposed to 5% SDS to fully denature the protein, and exposed for 30 min to a 0.5% solution of ^{18}O-labeled H_2O_2. Following chymotrypsin fragmentation, the $^{18}O/^{16}O$ ratio for each methionine residue was measured by mass spectrometry (*Materials and Methods*). For all three samples, the region exhibiting most substantial protection from initial ^{16}O-H_2O_2–mediated oxidation included methionine residues 322, 323, 336, 337, and 339. (*B*) The location of the footprinted region of 18 amino acids is highlighted in yellow on the sequences of the TDP43 LC domains of 11 vertebrate species ranging from humans (*Homo*) to fish (*Danio*). The methionine residue numbers of human TDP43 are indicated on the top of the sequence.

domains of 11 vertebrate species, ranging from fish to humans (Fig. 3*B*). The footprinted region colocalizes with an ultraconserved segment of 22 amino acids. In the 500 million years separating fish from humans, not a single amino acid has been changed within this ultraconserved region in any of the 11 species included in this analysis.

The overlapping footprinted and ultraconserved regions of the TDP43 LC domain also colocalize with a cross-β structure described recently from cryo-EM and solid-state NMR studies of TDP43 LC domain polymers (23, 24). Highly related, dagger-like structures were independently resolved by cryo-EM methods for three different cross-β polymers formed from the TDP43 LC domain (Fig. 4). Structural overlap among the three independent fibrils was observed to initiate at proline residue 320 of the TDP43 LC domain and persist for 15 residues to tryptophan residue 334. In Fig. 4, we compare the methionine oxidation footprint described in this study with the cross-β structures resolved by the Eisenberg laboratory. The two methionine residues most protected from H_2O_2-mediated oxidation, M322 and M323, are disposed wholly within the cross-β structure. The moderately protected methionine residues M336, M337, and M339 are located on the immediate C-terminal side of the cross-β structure. Finally, all five of the oxidation-exposed residues of M307, M311, M359, M405, and M414 were located outside of the Eisenberg cross-β structure.

The potential roles of different methionine residues in helping establish the biological utility of the TDP43 LC domain were investigated by introducing methionine-to-valine (M-to-V) substitutions into the protein sequence. Each of the 10 M-to-V variants was expressed, purified, and tested in assays for liquid-like droplet formation and cross-β polymerization as deduced by thioflavin-T staining. Eight of the 10 M-to-V variants generated liquid-like droplets indistinguishable from droplets formed from the native LC domain of TDP43 (*SI Appendix*, Fig. S7*A*). The M337V variant produced smaller droplets that were noticeably less translucent than those formed by the native LC domain, and the M323V variant yielded amorphous aggregates instead of liquid-like droplets.

The cross-β polymerization capacity of the native LC domain of TDP43 was compared with that of the nine droplet-competent M-to-V variants under three conditions: 1) in the absence of H_2O_2-mediated oxidation; 2) following mild oxidation; and 3) following extensive oxidation. Partial and full oxidation reactions were carried out in the presence of 6 M guanidine such that oxidation would not be influenced by any form of protein structure (*Materials and Methods*). After quenching with sodium sulfite, samples were analyzed by SDS-PAGE to ensure equivalent levels of protein integrity and degree of oxidation (Fig. 5*A*). Polymerization was initiated via dilution out of 6 M guanidine and monitored by spectrophotometry using thioflavin-T fluorescence (Fig. 5*B*). In the absence of oxidation, all nine variants were observed to polymerize as rapidly as the native LC domain, with mildly enhanced polymerization observed for the M336V, M337V, and M339V variants. Under saturating conditions of H_2O_2-mediated oxidation, none of the 10 proteins displayed any evidence of polymerization (*SI Appendix*, Fig. S7*B*). Finally, under conditions of partial oxidation, no polymerization was observed for the native TDP43 LC domain. Mild oxidation similarly prevented polymerization for six of the M-to-V variants. Surprisingly, the M337V variant and, to lesser extents, the M336V and M339V variants, polymerized despite partial oxidation.

Discussion

Here, we describe studies of the low complexity domain of the TDP43 protein. We offer the following observations pertinent to the study of this protein. First, the LC domain of TDP43 assembles into a cross-β structure that accounts for localized protection from H_2O_2-mediated oxidation. The morphological properties of the observed pattern of oxidation protection yield a footprint that is similar whether taken from highly polymerized, hydrogel samples of the protein, liquid-like droplet samples of the protein, or the TDP43 protein endogenous to living cells (Fig. 3).

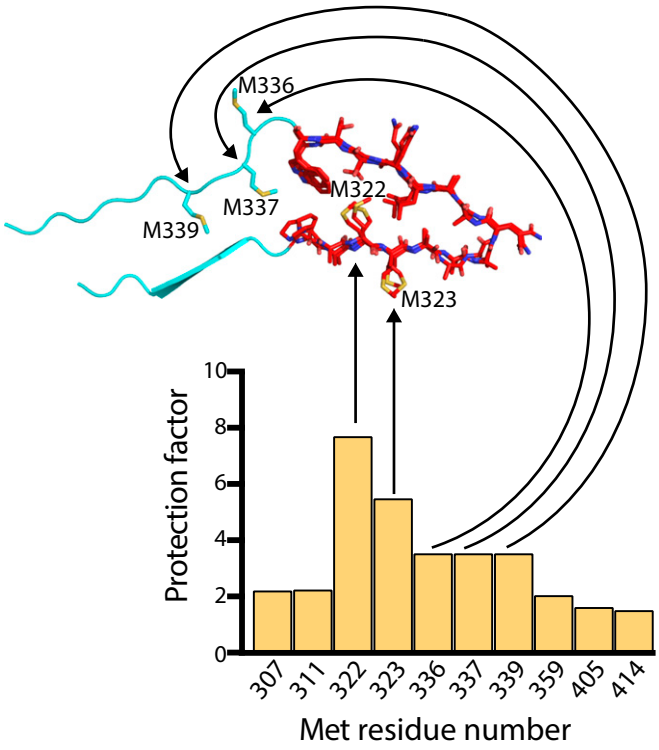

Fig. 4. Correspondence of TDP43 LC domain oxidation footprint and molecular structure of cross-β polymers as deduced by cryo-EM. Arrows connect methionine residues protected from H_2O_2-mediated oxidation (TDP43 LC domain hydrogel footprint) with their position either within the cross-β polymer core (M322 and M323), or on the immediate, C-terminal side of the polymer core (M336, M337, and M339). Molecular model of TDP43 LC domain polymer core is derived from cryo-EM structures resolved for three independent TDP43 LC domain fibrils (23).

Second, the location of this footprinted region of the TDP43 LC domain corresponds precisely to a region of extreme evolutionary conservation (Fig. 3). The footprinted region is also coincident in location to that of a cross-β polymer core of the TDP43 LC domain characterized at a molecular level by cryo-EM (Fig. 4) (23). Indeed, the idiosyncratic properties of the TDP43 LC domain footprint correlate with the molecular structure of the cross-β polymers resolved by Eisenberg and coworkers. Some degree of transient confusion may, however, accompany publication of the present work because Eisenberg's dagger-like polymers were reported to be assembled irreversibly (23), whereas our polymers are readily disassembled upon exposure to hydrogen peroxide or assayed by semi-denaturating detergent agarose gel electrophoresis (*SI Appendix*, Figs. S1 and S2). Nonetheless, it is our belief that our TDP43 LC domain polymers are likely to be assembled in a manner analogous to Eisenberg's dagger-like structures.

Our observations are not easily reconciled with the reported presence of localized α-helical structure within the TDP43 LC domain (9, 10, 25–27). Solution NMR spectroscopic measurements have given evidence of α-helical secondary structure between residues 322 and 344 of the LC domain in a limited population of TDP-43 molecules. Intriguingly, it is this same region that has been shown to: 1) form structurally precise cross-β interactions at physiological pH (7.4–7.5) as deduced by both cryo-EM and solid-state NMR approaches (23, 24, 28); 2) be protected in a structure-dependent manner from H_2O_2-mediated oxidation (Fig. 3*A*); and 3) be strikingly conserved through evolution (Fig. 3*B*). All of the five reports describing this α-helical structure made note that the helix was partially observed only under conditions of acidic pH (lower than 6.1). In two of the five studies, under near-neutral pH (6.5 and above), the TDP43 LC domain was observed to quickly adopt secondary structure heavily dominated by β-conformation (9, 27).

Given that the locations of the α-helical and β-enriched structures of the TDP43 LC domain precisely colocalized, they cannot coexist. Knowing that intracellular pH is neutral, not acidic, we predict that the TDP43 LC domain prefers to adopt a β-conformation in living cells. To this end, we make note that our methionine oxidation footprints observed at neutral pH were indistinguishable as visualized in hydrogel polymers of the TDP43 LC domain (which undoubtedly exist in a cross-β structural conformation), liquid-like droplets, and living cells (Fig. 3).

The third observation of note presented in this study is that M-to-V mutation of residues 336, 337, and 339 of the TDP43 LC domain yielded proteins that polymerize more rapidly than normal and are partially resistant to H_2O_2-mediated inhibition of polymerization (Fig. 5). We make note that the M337V mutation has been observed in independent kindreds by human genetic studies of ALS (29, 30) and that CRISPR-mediated introduction of this single amino acid change into the endogenous TDP43 gene of mice leads to profound neuropathology (31, 32).

We hypothesize that methionine residues 336, 337, and 339 may be of particular importance to a "redox switch" evolutionarily crafted into the LC domain of TDP43. Whereas methionine residues located outside of the cross-β core of the LC domain are far easier to oxidize than those located proximal to the polymer core, we imagine that oxidation of "easy-to-hit" methionine residues may trigger a cascade that loosens the structure—eventually allowing for oxidation of methionine residues 336, 337, and/or 339. Once oxidized within the four amino acid region specifying these "cardinal" methionine residues, we offer that polymerization of the TDP43 LC domain is effectively blocked until the MsrA and MsrB methionine sulfoxide reductase enzymes are able to reduce the protein and revive capacity for LC domain self-association.

Extending from these thoughts, it is possible to appreciate the potential hazard of the M337V mutation, as it might aberrantly allow sustained cytoplasmic aggregation of TDP43 under conditions of partial oxidation. Oxidation-resistant self-assembly of the TDP43 LC domain by the M337V variant might result from a more tightly assembled cross-β structure as hinted by the polymerization assays shown in Fig. 5. It is likewise possible that replacement of methionine 337 with an amino acid side chain that is not susceptible to oxidation also contributes to oxidation resistance of the cross-β assembly. Either or both of these alterations in function of the TDP43 LC domain might account for the disease-causing penetrance of the M337V mutation (29, 30).

In many regards, the observations articulated herein parallel similar studies of the low complexity domain of the yeast ataxin-2 protein (16, 17). Those studies provided evidence that the 24 methionine residues within the yeast ataxin-2 LC domain engender redox sensitivity via the same mechanisms described herein for TDP43. The biologic utility of the yeast ataxin-2 redox sensor can be understood from comprehensive studies of that system. Yeast ataxin-2 is required for the metabolic state of mitochondria to be properly coupled to the TOR pathway and autophagy (17). Since the yeast ataxin-2 protein forms a cloud-like structure surrounding mitochondria, it is sensible to imagine that its methionine-rich LC domain is proximally poised to sense the presence or absence of mitochondria-generated reactive oxygen species. Indeed, detailed experiments have been undertaken to validate the importance of oxidation-mediated changes in the polymeric state of the yeast ataxin-2 LC domain as a key

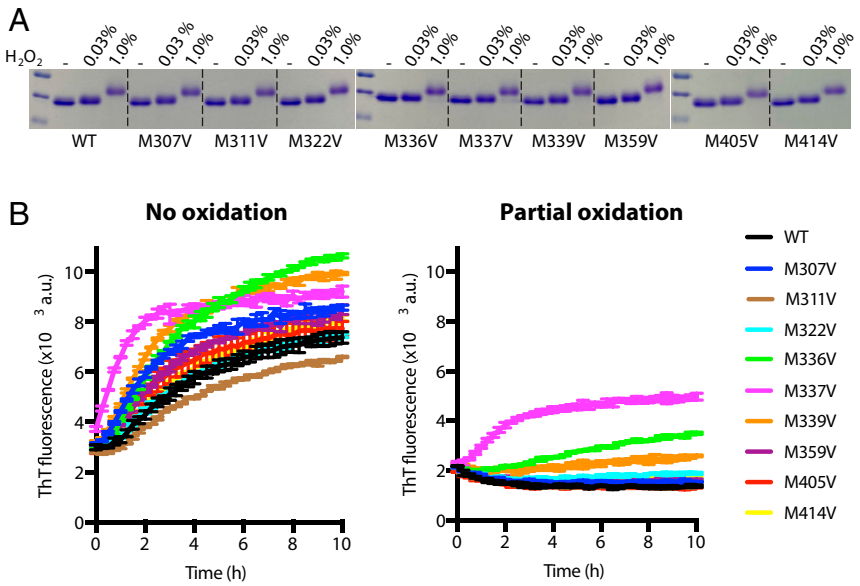

Fig. 5. Polymerization assays for nine M-to-V variants within the TDP43 LC domain. (*A*) Recombinant protein samples were prepared from the native (WT) TDP43 LC domain and nine M-to-V variants. Samples were prepared in the reduced state (–) as well as after exposure for 25 min to either 0.03% (partially oxidized) or 1% (heavily oxidized) H_2O_2 in the presence of 6 M guanidine HCl. The reduced, partially oxidized, and heavily oxidized samples of each protein were resolved by SDS-PAGE. (*B*) Oxidation reactions were quenched with sodium sulfite, and polymerization was monitored by thioflavin-T (ThT) fluorescence immediately following 20× dilution into polymerization buffer (*Materials and Methods*). All 10 of the reduced samples exhibited robust evidence of polymerization, with the M337V variant reproducibly exhibiting an enhanced rate of polymerization (*Left*). Upon partial oxidation resulting from exposure to 0.03% H_2O_2, polymerization was substantially inhibited for all samples save for the M337 variant (*Right*). No evidence of polymerization was observed for the native protein or any of the nine M-to-V variants subsequent to exposure to 1% H_2O_2 (*SI Appendix*, Fig. S7*B*).

event in coupling the metabolic state of mitochondria to the activity state of TOR and its influence on autophagy (17).

Unlike yeast ataxin-2, TDP43 is primarily a nuclear protein. Why, then, would the LC domain of TDP43 be endowed with the apparent capacity to sense reactive oxygen species? We speculate that when TDP43 shuttles out of the nucleus as a part of ribonucleoprotein complexes housed within RNA granules, oxidation-sensitive self-association of its LC domain might allow for the "unfurling" of RNA granules in the proximity of mitochondria. This might facilitate localized translation of certain mRNAs in the proximity of mitochondria, perhaps useful for optimizing synthesis of mitochondria-destined proteins in the immediate vicinity of mitochondria.

How might this redox regulation be supported by physiological levels of oxidants? The half-maximal concentration of H_2O_2 required for melting droplets of the TDP43 LC domain in vitro is roughly 0.2% (~60 mM) (estimated from Fig. 1*B*) vs. 0.33% (~100 mM) for the yeast ataxin-2 LC domain (16). These are indeed very high H_2O_2 concentrations. For yeast ataxin-2, we have observed that the addition of as little as 0.0025% H_2O_2 to yeast cells can result in inhibition of the protein's function (i.e., inhibition of autophagy) (16). This is the equivalent of ~0.7 mM H_2O_2. We speculate that local production of H_2O_2 within particular microcompartments in the cell (e.g., proximal to mitochondria-rich domains) could result in a much higher effective local H_2O_2 concentrations that are comparable to the concentration used in our studies. Lastly, we suspect that even partial oxidation of key methionine residues may be sufficient to tip the balance between monomeric and polymeric states (Fig. 5*B*). Based on these considerations, we predict that TDP43 LC domain may also be responsive to physiological levels of oxidants in cells.

The ability of MsrA and MsrB to reduce methionine sulfoxides in TDP43 and reverse its aggregation state may be pertinent to age-related alterations that occur in these enzymes. In this regard, it is notable that the accumulation of methionine sulfoxides and reductions in the activity of the Msr enzymes are well-described hallmarks of aging and age-related neurodegenerative disorders (33). It is, thus, possible that aging may disrupt regulation of the TDP43 "redox switch" and that this dysregulation may play a role in exacerbating the pathological features of aging and some neurodegenerative disorders.

We close with consideration of the prominent role of TDP43 in neuronal granules (4, 6). Neuronal granules are found in dendritic extensions of neurons where they are understood to facilitate localized translation proximal to active synapses (34). Knowing that active synapses are mitochondria-rich (35), we offer the simplistic idea that the LC domain of TDP43 might suffer enhanced oxidation upon encountering mitochondria-enriched synapses. If so, we further hypothesize that oxidation-induced dissolution of cross-β polymers otherwise adhering TDP43 to neuronal granules and their resident mRNAs might assist in facilitating synapse-proximal translation.

Materials and Methods

Phase-Separated Droplet Formation. Phase-separated droplets of His-TDP43 LC domain were formed by a quick dilution of the purified protein out of denaturing conditions into gelation buffer containing 25 mM Tris pH 7.5, 200 mM NaCl, 10 mM β-mercaptoethanol, and 0.5 mM EDTA to reach the final protein concentration of 10–20 μM. Images of liquid-like droplets were taken using Bio-Rad ZOE Fluorescent Cell Imager.

H_2O_2-Mediated Melting of Phase-Separated Liquid-like Droplets. Liquid-like droplet solutions were incubated for 30 min at room temperature. H_2O_2 was added to the droplet solution to obtain final concentrations of 0.003% (0.98 mM), 0.006% (1.98 mM), 0.01% (3.3 mM), 0.02% (6.6 mM), 0.03% (9.8 mM), 0.06% (19.8 mM), 0.1% (33 mM), 0.2% (66 mM), 0.3% (98 mM), 0.6% (198 mM), and 1% (330 mM). After 1 h incubation at room temperature, droplets images were taken using a Bio-Rad ZOE Fluorescent Cell Imager. To visualize protein oxidation caused by H_2O_2, a portion of the reaction mixture was recovered and analyzed by SDS-PAGE.

Enzymatic Reduction of H_2O_2-Oxidized Protein by Methionine Sulfoxide Reductase Enzymes. Liquid-like droplets of His-tagged TDP43 LCD (100 μL) were first formed as described above. Solutions were transferred into a 96-well plate and droplets melted by adding H_2O_2 to a final concentration of 0.5% (165 mM). After droplets completely disappeared, 3 μL of 2 M Na_2SO_3 was added to the mixture in order to quench residual H_2O_2. After incubation for 1 h, 2.5 mM NADPH solution was added. Subsequently, 10 μL of a 10× enzyme mixture mix that contained 1 μM MBP-MsrA, 10 μM MBP-MsrB, 100 μM His-tagged Trx1, and 20 μM His-tagged Trr1 was added. The reaction mixture was incubated at room temperature and inspected for droplet revival. Images were taken with Bio-Rad ZOE Fluorescent Cell Imager after incubation overnight. To visualize protein reduction, a portion of the reaction mixture was recovered from the well and analyzed by SDS-PAGE.

Mammalian Cell Culture and Generation of HEK293 Cells Harboring CRISPR-Edited TDP43. Mammalian cell culture experiments were performed using the HEK293 cell line (American type culture collection). For site-specific integration of the 3×Flag-GFP into the endogenous TDP43 locus, three sgRNAs were designed to target regions close to the TDP43 start codon and cloned into pGuide-it vector (TaKaRa) using published methods (36). To construct the donor vector, ∼1,000-bp homologous arms located upstream or downstream from the TDP43 start codon were amplified by PCR. The 3×Flag-GFP sequence was also PCR amplified. The three DNA pieces, upstream of TDP43 start codon, 3×Flag-GFP, and downstream, were introduced into pGEM-T Easy vector by In-Fusion cloning (TaKaRa). HEK293 cells were cotransfected with the donor vector and small guide RNAs using Lipofectamine 2000 (Thermo Fisher Scientific). Posttransfection, cells were split at low density to allow formation of single colonies. GFP-positive colonies containing properly inserted 3×Flag-GFP were screened by anti-Flag Western blotting and confirmed by DNA sequencing.

Sample Preparation for In Vitro Footprinting. Three protein samples were prepared: 1) the TDP43 LCD in a highly polymeric, hydrogel form; 2) the TDP43 LCD in the liquid-like droplet form; and 3) the TDP43 LCD in the monomeric form (denatured in 6 M guanidine HCl). To obtain TDP43 LCD polymers, His-TDP43 LCD purified in 6 M guanidine buffer was diluted to 100 μM in gelation buffer containing 25 mM Tris pH 7.5, 200 mM NaCl, 10 mM β-ME, and 0.5 mM EDTA and left at room temperature for 2 d. For the denatured sample, purified His-tagged TDP43 LCD was dialyzed in denaturing buffer containing 25 mM Tris·HCl pH 7.5, 200 mM NaCl, 6 M guanidine HCl, 10 mM fresh β-ME, and concentrated to 100 μM. For liquid-like droplet formation, purified His-TDP43 LCD in 6 M guanidine buffer was diluted to 100 μM in gelation buffer leading to immediate formation of liquid-like droplets.

All samples were oxidized by ^{16}O-labeled H_2O_2 at concentrations of 0%, 0.03%, 0.1%, 0.25%, and 0.5% for 30 min. Oxidation reactions were quenched by the addition of twice the molar ratio of Na_2SO_3 relative to H_2O_2. All samples were then denatured in buffer containing 25 mM Tris pH 7.5, 200 mM NaCl, 6 M guanidine HCl, 10 mM fresh β-ME. To remove H_2O_2 and Na_2SO_3, buffer was exchanged using a centrifugal filter (Millipore). To achieve full oxidation, 0.5% ^{18}O-labeled H_2O_2 was added to the samples, allowing further oxidation for 30 min. Reactions were quenched by addition of twice the molar ratio of Na_2SO_3, then processed for mass spectrometry.

Sample Preparation for In Vivo Footprinting. Ten 15-cm dishes of HEK293 3×Flag-GFP CRISPR cells were prepared for each assay point. At ∼80% confluency, cells were treated with four concentrations of ^{16}O-labeled H_2O_2, 0%, 0.01%, 0.03%, 0.1% for 5 min at 37 °C. Cells were harvested, frozen in liquid nitrogen, ground by cryomill (Restch), and resuspended in IP buffer (20 mM Hepes pH 7.4, 100 mM Na_2PO_4, 50 mM Na Citrate, 100 mM NaCl, 0.1% Tween 20, 4 M urea). After brief sonication, the cell lysate was centrifuged at 13,400 rpm for 10 min at 4 °C. Supernatant was diluted fivefold in lysis buffer without urea (20 mM Hepes pH 7.4, 100 mM Na_2PO_4, 50 mM Na Citrate, 100 mM NaCl, 0.1% Tween 20), followed by anti-Flag-immunoprecipitation (IP). Cell lysate was bound to Flag beads, washed three times with IP buffer, and eluted at 95 °C in buffer supplemented with 5% SDS. A solution composed of elution buffer supplemented with 0.5% ^{18}O-H_2O_2 was added to each sample to effect full oxidation and, after 30 min, quenched with twice the molar ratio of Na_2SO_3. Buffer exchange was then performed to move samples into a solution compatible with mass spectrometry (50 mM triethylammonium bicarbonate, 5% SDS).

Additional information on the experimental methods can be found in *SI Appendix*.

Data Availability. All study data are included in the article and supporting information.

ACKNOWLEDGMENTS. We thank Deepak Nijhawan for thoughtful discussions regarding the research described herein. S.L.M. was supported by National Institute of General Medical Sciences Grant 5R35GM13130358 as well as unrestricted funding from an anonymous donor. S.G. was supported by National Institute of General Medical Sciences Grant 5R35GM13130358. B.P.T. was supported by National Institute of Neurological Disorders and Stroke Grant RO1NS115546, funding provided by University of Texas Southwestern Medical Center as a Presidential Scholar and funding from the Howard Hughes Medical Institute as a Faculty Scholar.

1. E. B. Lee, V. M. Lee, J. Q. Trojanowski, Gains or losses: Molecular mechanisms of TDP43-mediated neurodegeneration. *Nat. Rev. Neurosci.* **13**, 38–50 (2011).
2. M. Neumann *et al*., Ubiquitinated TDP-43 in frontotemporal lobar degeneration and amyotrophic lateral sclerosis. *Science* **314**, 130–133 (2006).
3. E. Buratti *et al*., Nuclear factor TDP-43 and SR proteins promote in vitro and in vivo CFTR exon 9 skipping. *EMBO J.* **20**, 1774–1784 (2001).
4. P. P. Gopal, J. J. Nirschl, E. Klinman, E. L. Holzbaur, Amyotrophic lateral sclerosis-linked mutations increase the viscosity of liquid-like TDP-43 RNP granules in neurons. *Proc. Natl. Acad. Sci. U.S.A.* **114**, E2466–E2475 (2017).
5. E. Buratti, F. E. Baralle, The multiple roles of TDP-43 in pre-mRNA processing and gene expression regulation. *RNA Biol.* **7**, 420–429 (2010).
6. J. F. Chu, P. Majumder, B. Chatterjee, S. L. Huang, C. J. Shen, TDP-43 regulates coupled dendritic mRNA transport-translation processes in co-operation with FMRP and Staufen1. *Cell Rep.* **29**, 3118–3133.e6 (2019).
7. M. Mompeán *et al*., The TDP-43 N-terminal domain structure at high resolution. *FEBS J.* **283**, 1242–1260 (2016).
8. A. S. Chen-Plotkin, V. M. Lee, J. Q. Trojanowski, TAR DNA-binding protein 43 in neurodegenerative disease. *Nat. Rev. Neurol.* **6**, 211–220 (2010).
9. L. Lim, Y. Wei, Y. Lu, J. Song, ALS-causing mutations significantly perturb the self-assembly and interaction with nucleic acid of the intrinsically disordered prion-like domain of TDP-43. *PLoS Biol.* **14**, e1002338 (2016).
10. A. E. Conicella, G. H. Zerze, J. Mittal, N. L. Fawzi, ALS mutations disrupt phase separation mediated by α-helical structure in the TDP-43 low-complexity C-terminal domain. *Structure* **24**, 1537–1549 (2016).
11. E. Buratti, Functional significance of TDP-43 mutations in disease. *Adv. Genet.* **91**, 1–53 (2015).
12. M. P. Hart, A. D. Gitler, ALS-associated ataxin 2 polyQ expansions enhance stress-induced caspase 3 activation and increase TDP-43 pathological modifications. *J. Neurosci.* **32**, 9133–9142 (2012).
13. G. Y. Hsiung *et al*., Clinical and pathological features of familial frontotemporal dementia caused by C9ORF72 mutation on chromosome 9p. *Brain* **135**, 709–722 (2012).
14. M. Kato *et al*., Cell-free formation of RNA granules: Low complexity sequence domains form dynamic fibers within hydrogels. *Cell* **149**, 753–767 (2012).
15. S. Xiang *et al*., The LC domain of hnRNPA2 adopts similar conformations in hydrogel polymers, liquid-like droplets, and nuclei. *Cell* **163**, 829–839 (2015).
16. M. Kato *et al*., Redox state controls phase separation of the yeast ataxin-2 protein via reversible oxidation of its methionine-rich low-complexity domain. *Cell* **177**, 711–721.e8 (2019).
17. Y. S. Yang *et al*., Yeast ataxin-2 forms an intracellular condensate required for the inhibition of TORC1 signaling during respiratory growth. *Cell* **177**, 697–710.e7 (2019).
18. Y. Lin *et al*., Toxic PR poly-dipeptides encoded by the C9orf72 repeat expansion target LC domain polymers. *Cell* **167**, 789–802.e12 (2016).
19. J. Moskovitz, B. S. Berlett, J. M. Poston, E. R. Stadtman, The yeast peptide-methionine sulfoxide reductase functions as an antioxidant in vivo. *Proc. Natl. Acad. Sci. U.S.A.* **94**, 9585–9589 (1997).
20. E. J. Walker, J. Q. Bettinger, K. A. Welle, J. R. Hryhorenko, S. Ghaemmaghami, Global analysis of methionine oxidation provides a census of folding stabilities for the human proteome. *Proc. Natl. Acad. Sci. U.S.A.* **116**, 6081–6090 (2019).
21. H. J. Wobst *et al*., Cytoplasmic relocalization of TAR DNA-binding protein 43 is not sufficient to reproduce cellular pathologies associated with ALS *In vitro*. *Front. Mol. Neurosci.* **10**, 46 (2017).
22. C. Appocher *et al*., Major hnRNP proteins act as general TDP-43 functional modifiers both in Drosophila and human neuronal cells. *Nucleic Acids Res.* **45**, 8026–8045 (2017).
23. Q. Cao, D. R. Boyer, M. R. Sawaya, P. Ge, D. S. Eisenberg, Cryo-EM structures of four polymorphic TDP-43 amyloid cores. *Nat. Struct. Mol. Biol.* **26**, 619–627 (2019).
24. X. F. Zhuo *et al*., Solid-state NMR reveals the structural transformation of the TDP-43 amyloidogenic region upon fibrillation. *J. Am. Chem. Soc.* **142**, 3412–3421 (2020).

25. A. E. Conicella *et al*., TDP-43 α-helical structure tunes liquid-liquid phase separation and function. *Proc. Natl. Acad. Sci. U.S.A.* **117**, 5883–5894 (2020).
26. H. R. Li *et al*., The physical forces mediating self-association and phase-separation in the C-terminal domain of TDP-43. *Biochim. Biophys. Acta. Proteins Proteomics* **1866**, 214–223 (2018).
27. L. L. Jiang *et al*., Structural transformation of the amyloidogenic core region of TDP-43 protein initiates its aggregation and cytoplasmic inclusion. *J. Biol. Chem.* **288**, 19614–19624 (2013).
28. J. Shenoy *et al*., Structural dissection of amyloid aggregates of TDP-43 and its C-terminal fragments TDP-35 and TDP-16. *FEBS J.* **287**, 2449–2467 (2019).
29. A. Tamaoka *et al*., TDP-43 M337V mutation in familial amyotrophic lateral sclerosis in Japan. *Intern. Med.* **49**, 331–334 (2010).
30. N. J. Rutherford *et al*., Novel mutations in TARDBP (TDP-43) in patients with familial amyotrophic lateral sclerosis. *PLoS Genet.* **4**, e1000193 (2008).
31. D. Gordon *et al*., Single-copy expression of an amyotrophic lateral sclerosis-linked TDP-43 mutation (M337V) in BAC transgenic mice leads to altered stress granule dynamics and progressive motor dysfunction. *Neurobiol. Dis.* **121**, 148–162 (2019).
32. S. Y. Ebstein, I. Yagudayeva, N. A. Shneider, Mutant TDP-43 causes early-stage dose-dependent motor neuron degeneration in a TARDBP knockin mouse model of ALS. *Cell Rep.* **26**, 364–373.e4 (2019).
33. B. C. Lee, V. N. Gladyshev, The biological significance of methionine sulfoxide stereochemistry. *Free Radic. Biol. Med.* **50**, 221–227 (2011).
34. M. A. Kiebler, G. J. Bassell, Neuronal RNA granules: Movers and makers. *Neuron* **51**, 685–690 (2006).
35. M. J. Devine, J. T. Kittler, Mitochondria at the neuronal presynapse in health and disease. *Nat. Rev. Neurosci.* **19**, 63–80 (2018).
36. F. A. Ran *et al*., Genome engineering using the CRISPR-Cas9 system. *Nat. Protoc.* **8**, 2281–2308 (2013).